Science Advances
AAAS

Supplementary Materials for

Caribbean salinity anomalies contributed to variable North Atlantic circulation and climate during the Common Era

Anastasia Zhuravleva *et al.*

Corresponding author: Anastasia Zhuravleva, anastasia.zhuravleva@dal.ca; Henning A. Bauch, hbauch@geomar.de

Sci. Adv. **9**, eadg2639 (2023)
DOI: 10.1126/sciadv.adg2639

The PDF file includes:

Supplementary Text
Figs. S1 to S7
Tables S1 to S4
References

Other Supplementary Material for this manuscript includes the following:

Data S1 and S2

Supplementary Text

Comparison with the nearby core-top SST estimates

As can be seen from table S2, our SST estimate for the M35003-6 core-top is ~1.3±0.5 °C lower than previously obtained for this location (53) and for a core M35/1-2-1 that is 10 km apart (21). While these previous studies examined only larger specimens (>250 µm; ref. 21,53), we analyzed a large variety of *G. ruber* (white) shell sizes (>150 µm), including also small individuals that tend to prevail during the winter season (61). Therefore, the slightly colder core-top SST obtained here can be the result of either different calcification rates or seasonal preferences. Despite some discrepancies, all core-top SST and SSS estimates are consistent with the mean annual temperature and salinity of the upper water column in the Tobago Basin (Fig. 3 in the main text).

Age model

Dating of Caribbean cores is currently associated with centennial-scale age errors, due to uncertainties in both radiocarbon calibration and local marine reservoir correction (ΔR) values (62,63). Additional errors in the range of decades to centuries may result from the ΔR variability associated with changes in Orinoco and Amazon discharges (63) and bioturbation. However, accurate age control in our sedimentary archive is essential to investigate the covariance (or lack thereof) between the southeastern Caribbean and Gulf of Mexico SSS.

The initial age model for core M35003-6 was based on four ^{14}C accelerator mass spectrometer (AMS) dates using *G. ruber* (white). The dating was carried out at Leibniz Laboratory for Radiometric Dating and Stable Isotope Research, Kiel, Germany (fig. S2; table S3). The AMS ^{14}C

ages were calibrated using *RBacon* (64) and a recent Marine20 calibration curve with a modern global ocean age increased by ~150 years when compared to 400 years previously used in Marine13 (62). The ΔR value was taken from the ΔR database updated for Marine20 (http://calib.org/marine) by averaging values from 7 nearest points in the southeastern Caribbean region (-248±144 years, Trinidad, Tobago, Los Testigos; refs. 63,65). The high positive value from Grenada (282±24 years, ref. 63) was not included in our calculation, because samples associated with the Atlantic influence tend to have strongly negative values (63,65,66). In addition, a modern age for the core-top was assumed because our box core contained an intact and excellently preserved sediment-water interface. We note, however, that the resulting age model suggests constant sedimentation rates over the past 2,000 years (fig. S2), which is not supported by our sedimentological data. In particular, high number of coarse lithic grains (>150 µm) at the base of our box core (lower ~10 cm) indicates lowered deposition of fine-grained fluvial material (fig. S2), and, therefore, a pronounced change in sedimentation rates is expected, in agreement with earlier reconstructions at this site (e.g., ref. 20).

To account for the unavoidable dating ambiguity resulting from both radiocarbon-date uncertainties and variable sedimentation rates, we build our chronology on alignment to the Gulf of Mexico SST record (core 2010-GB2-MCA, ref. 14). We updated the original age model for core 2010-GB2-MCA using the Marine20 ΔR database (ΔR=-164±9 years, ref. 66) and a Marine20 calibration curve (62). Paired Mg/Ca-$\delta^{18}O$ values from this core were reprocessed in PSU Solver (23) using the same calibrations as proposed in the original publication (14). Analytical and sampling uncertainties were incorporated into overall uncertainty derived in PSU Solver (for Mg/Ca, combined 2σ analytical and sampling uncertainty of ±0.10 mmol/mol; for $\delta^{18}O$, only 2σ analytical uncertainty of ±0.12 ‰). Each sampling depth was also associated with a 2σ age uncertainty of ±150 years based on radiocarbon dating (table S4). The estimated average 1σ (2σ) uncertainty is ±0.6 (1.1) °C for SST and ±0.3 (0.6) units for SSS.

To align Caribbean and Gulf of Mexico SST records, we make use of two climate events that are distinct in both records: 1) the pronounced SST cooling prior to the Medieval Peak Warmth and 2) the warmer spell of the LIA (fig. S2). Our assumption of synchronous SST changes across these two basins is based on observations (67) and correlation analysis (ref. 14, their fig. S3). By using the Gulf of Mexico SST record as a reference we assume that uncertainties in core 2010-GB2-MCA chronology are lower, which is justified e.g., by smaller errors in ΔR (66) and/or lower bioturbation effects. The latter is supported by radionuclide data showing that active sediment mixing on the seafloor in the oligotrophic Gulf of Mexico is limited to upper 4 cm (68). In contrast, the >8 cm thickness of bioturbated sediment layer in the southeastern Caribbean cannot be ruled out, due to its relatively high primary productivity and organic carbon flux under riverine fertilization (27,69). The resultant sedimentation rates over the last 1,700 years between ~10 and 45 cm kyr^{-1} are consistent with earlier reconstructions on the Holocene at this site (20,70). However, we suggest that the core section older than 550 C.E. is characterized by low sedimentation rates, based on high number of coarse grains indicative of reduced fluvial inputs. Due to the lack of adequate age control, we do not interpret this older part of the record.

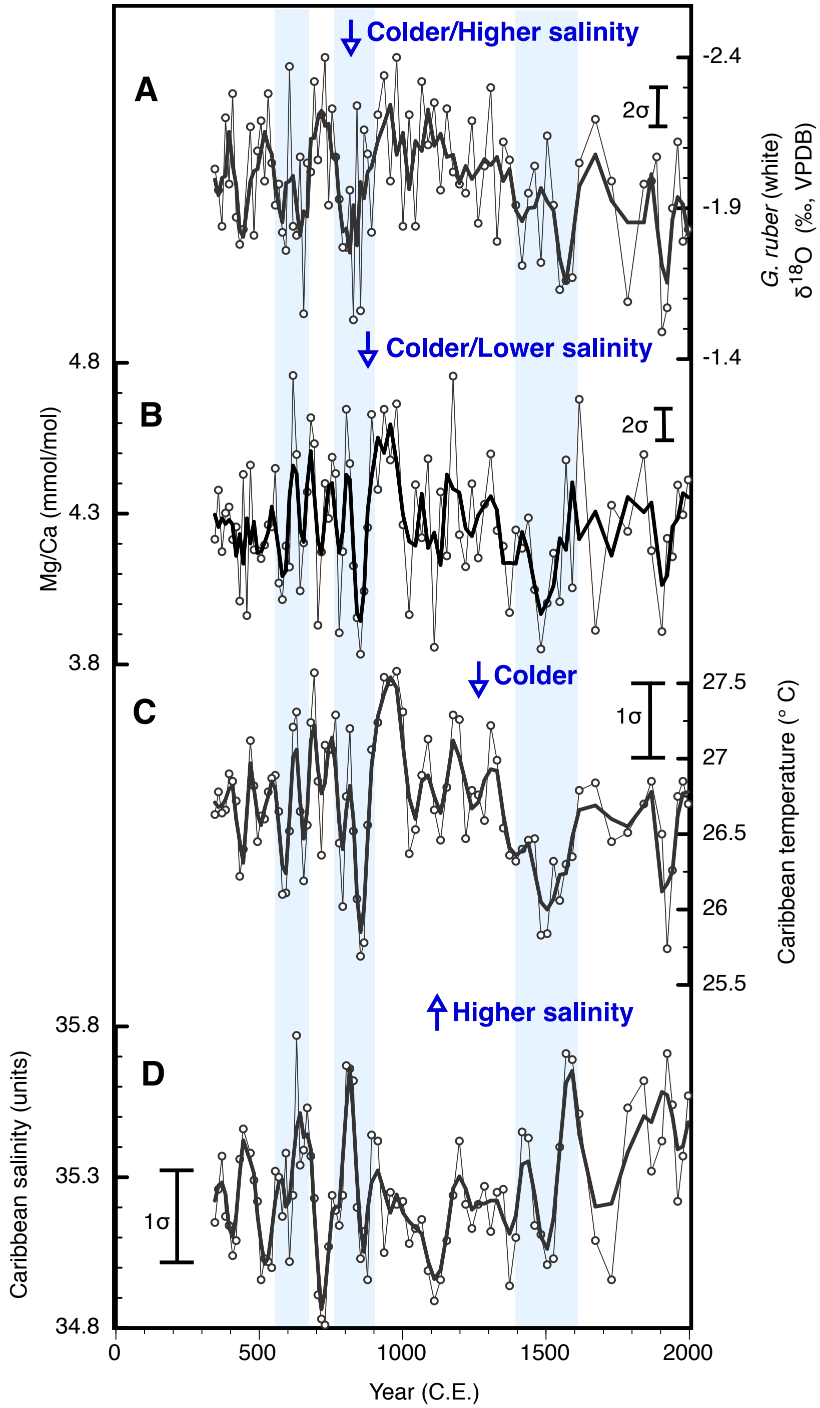

Fig. S1. Proxy data from core M35003-6 over the past 1,700 years. **(A, B)** $\delta^{18}O$ and Mg/Ca values in *G. ruber* (white) with their 2σ analytical and sampling uncertainties (see Materials and Methods). **(C, D)** Mg/Ca-$\delta^{18}O$-based SST and SSS records; ±1σ uncertainties calculated in PSU Solver (see Materials and Methods). Original and smoothed records (3-point moving average) are shown. Blue bars denote centennial cooling/salinification events in the southeastern Caribbean.

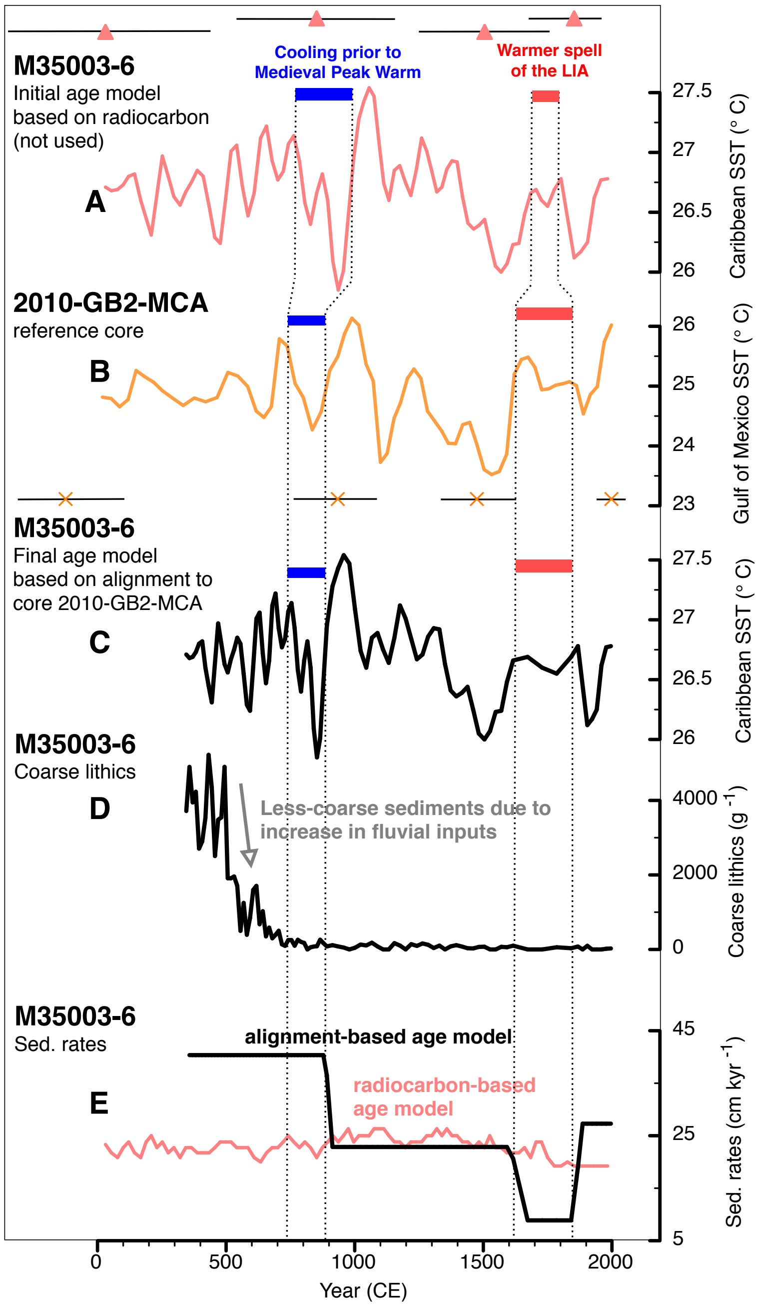

Fig. S2. Age model for core M35003-6. Smoothed (3-point moving average) SST record from core M35003-6 is plotted against timescales derived from **(A)** radiocarbon dates and **(C)** core-to-core correlations (i.e., the final age model). Dashed black lines show the alignment of M35003-6 SST record to **(B)** core 2010-GB2-MCA SST, smoothed using 2σ age model uncertainty in PSU Solver (14). Red triangles and orange crosses show calibrated radiocarbon dates (±2σ) for M35003-6 and 2010-GB2-MCA, respectively. Also shown is the abundance of lithic grains in the fraction >150 µm **(D)** and sedimentation rates in core M35003-6 **(E)**. Grey arrow in **(D)** denotes an abrupt reduction in the abundance of coarse lithic grains at c. 550 C.E. that must have coincided with an increase in fluvial inputs and, thus, higher sedimentation rates (see supplementary text). For radiocarbon dates and tie points, see tables S3 and S4.

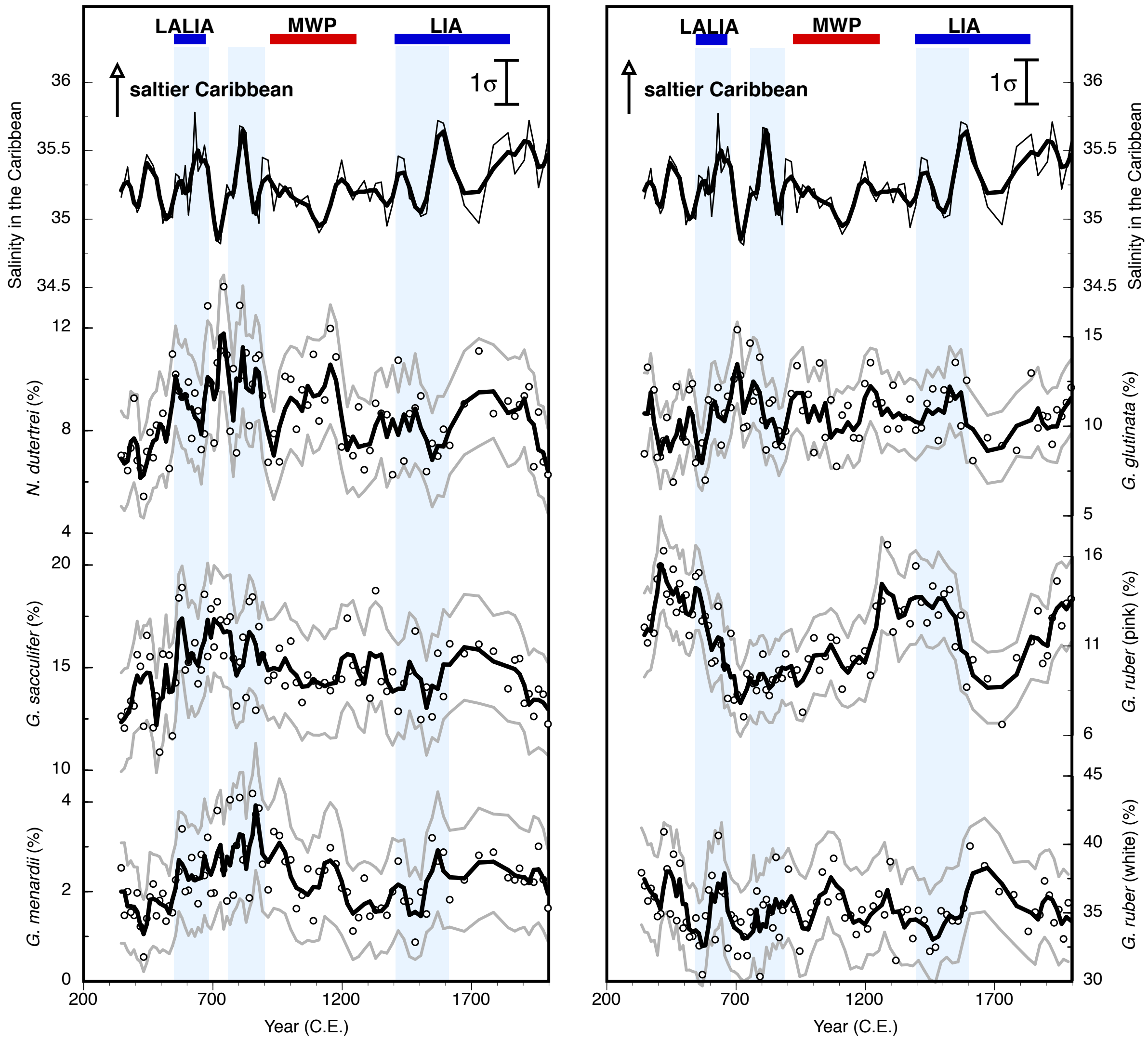

Fig. S3. Proportions of selected planktic foraminifera species in core M35003-6 compared to reconstructed sea-surface salinities (original and 3-point moving average smoothed records). For assemblage data, grey lines show 95 % confidence bounds for smoothed records (see Materials and Methods). Blue bars denote centennial cooling/salinification events in the southeastern Caribbean. LALIA – Late Antique Little Ice Age, LIA-Little Ice Age, MWP-Medieval Warm Period.

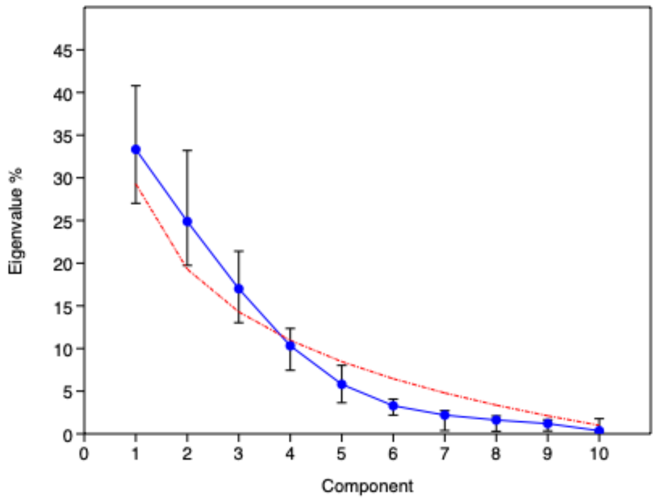

Fig. S4. Scree plot of the eigenvalues for the 10 principal components (PCs, blue line) of the Principal Component Analysis (PCA) performed on the planktic foraminifera assemblage dataset from core M35003-6. Error bars indicate the 95 % confidence interval computed by bootstrapping (n = 1000). PCs 1, 2, and 3 are considered significant, as the eigenvalues for these three PCs lie above the eigenvalues expected under a random model ("broken stick", red dashed line). We note, however, that the broken stick is inside the 95 % confidence interval for the fourth PC. PCA was performed using PAST software (48).

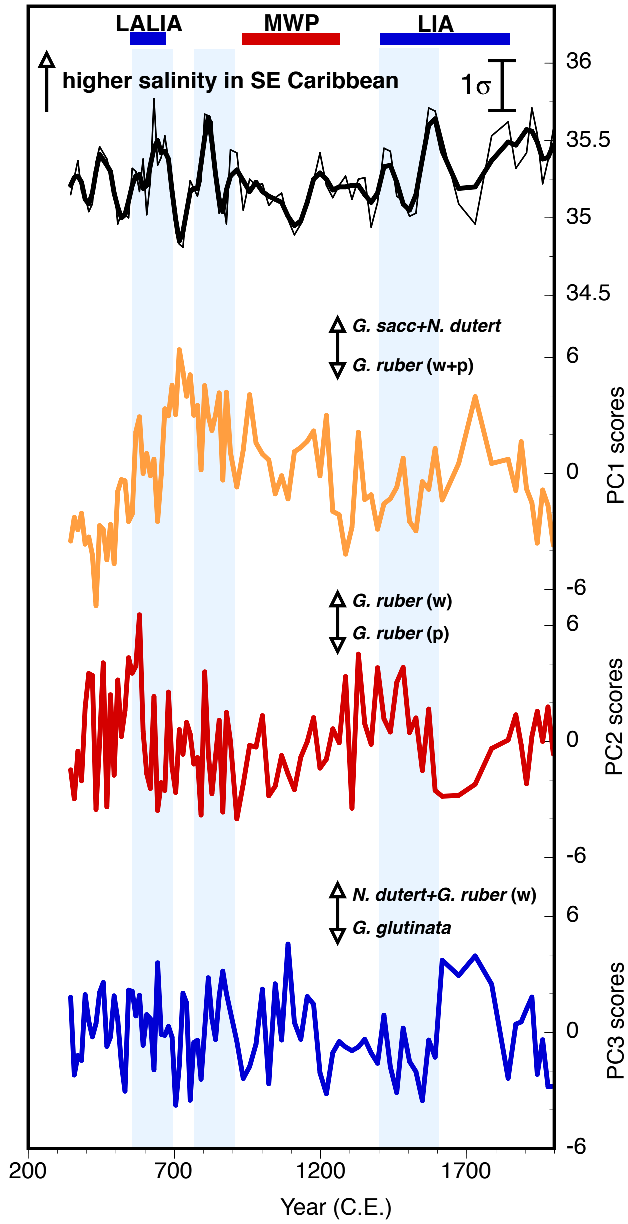

Fig. S5. Comparison between reconstructed salinities and scores of the principal components (PCs) of the planktic foraminifera assemblage dataset in core M35003-6. PC1 (orange line) explains 33 % of the dataset variance and shows high positive loadings for the proportions of *Globigerinoides sacculifer* and *Neogloboquadrina dutertrei* (0.43 and 0.34, respectively) and high negative coefficients for *Globigerinoides ruber* (pink) and *Globigerinoides ruber* (white) (-0.66 and -0.41, respectively). PC2 (red line) accounts for 27 % of the variance and represents a gradient between *G. ruber* (pink) (0.56) and *G. ruber* (white) (-0.63). PC3 (blue line, 17 % of the variance) represents a gradient where positive values represent the combined proportions of *G. ruber* (white) (0.42) and *N. dutertrei* (0.34) and negative values are associated with *G. glutinata* (-0.72). Correlations between the paleosalinity record and the scores of PCs 1-3 are insignificant ($p>0.05$). Blue bars denote centennial cooling/salinification events in the southeastern Caribbean. LALIA – Late Antique Little Ice Age, LIA-Little Ice Age, MWP-Medieval Warm Period.

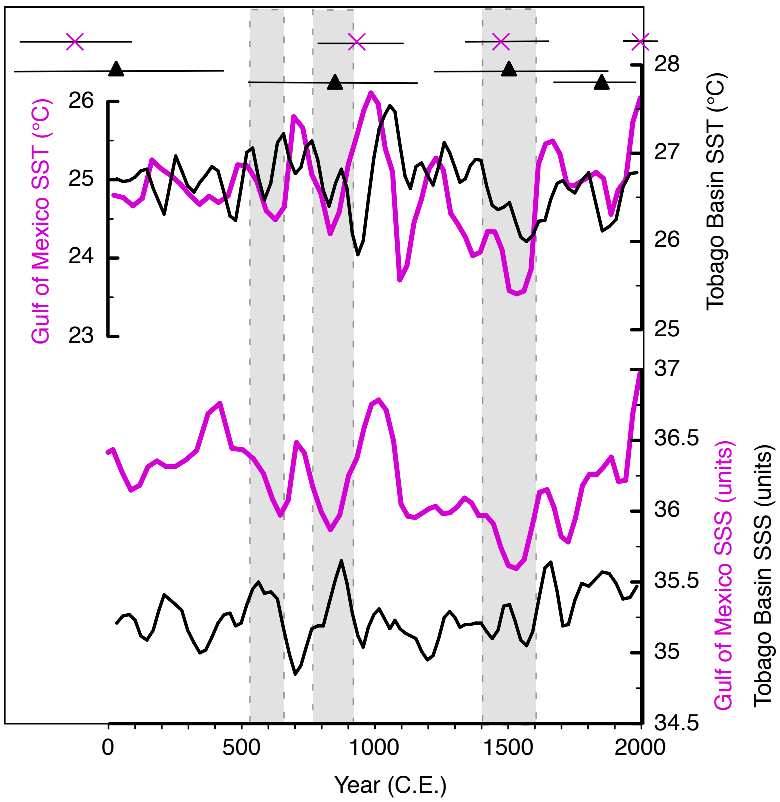

Fig. S6. Caribbean – Gulf of Mexico salinity seesaw on radiocarbon-derived timescales. Comparison of SST and SSS reconstructions from the Caribbean core M35003-6 (black, this study) and Gulf of Mexico core 2010-GB2-MCA (purple, ref. 14), plotted on the radiocarbon-based timescales. Black triangles and purple crosses show calibrated radiocarbon dates (±2σ) for M35003-6 and 2010-GB2-MCA, respectively. See supplementary text for details on the age model construction. For radiocarbon dates see tables S3 and S4. Grey bars denote centennial cooling/salinification events in the southeastern Caribbean as discussed in the main text.

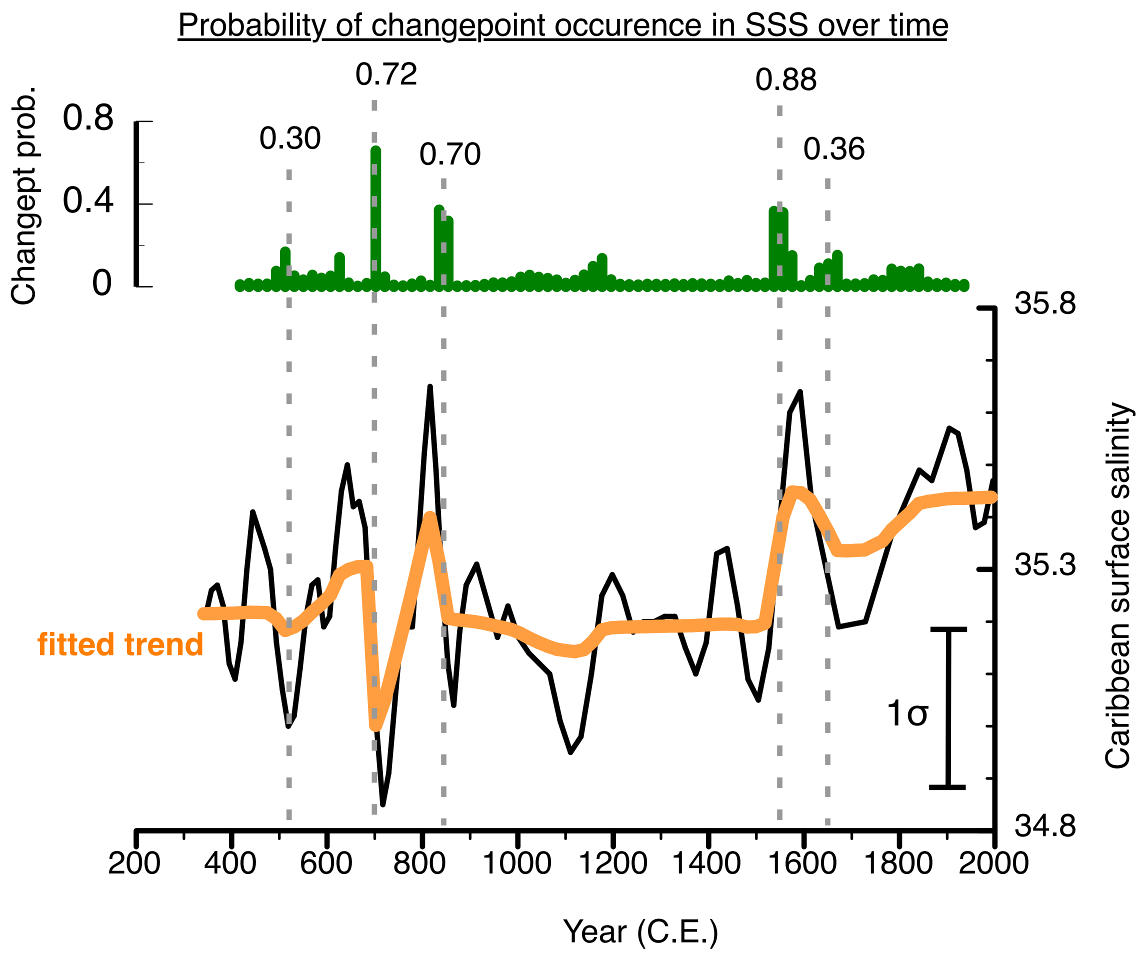

Fig. S7. BEAST decomposition of the sea surface salinity (SSS) reconstructed from core M35003-6. Smoothed (3-point moving average) SSS timeseries (black line) were decomposed into abrupt changes (green bars) and a fitted trend (orange line). The median number of changepoints in the SSS trend is five (12 % probability; dashed grey lines). Green bars show probability distribution of having a changepoint in the trend at each point of time. Higher peaks indicate a higher chance of being a changepoint only at that particular single point in time and does not necessarily mean a higher chance of observing a changepoint around that time. The summed probability for each change point is indicated with numbers. BEAST, a Bayesian change point detection algorithm (24), supports statistical significance of SSS changes between 550 and 900 C.E. and an increase in surface salinity at 1550 C.E.

Table S1. List of proxy records used in the study.

# in Fig. 1	Material	Location	Coordinates	Water depth	Reference
1	Box core M35003-6	Tobago Basin, southeastern Caribbean	12°05′06″N 61°14′42″W	1299 m	this study
2	Lacustrine sediment core	South Sawtooth Lake, Ellesmere Island, Canada	79°21′03″N 83°57′07″W	80 m (lake)	Ref. 15
3	*Arctica islandica* site	north Icelandic shelf	66°31′35″N 18°11′44″W	80 m	Refs. 12,13
4	RAPiD-35-COM (box core RAPiD-35-25B and piston core RAPiD-35-14P)	Eirik Drift, eastern Labrador Sea	Box core – 57°30′28″N 48°43′24″W Piston core – 57°30′15″ N 48°43′20″ W	~3485 m	Ref. 10
5	RAPiD-21-COM (box core RAPiD-21-12B and kasten core RAPiD-21-3K)	Gardar Drift, subpolar North Atlantic	Box core – 57°27′05″N 27°54′14″W Kasten core – 57°27′05″N 27°54′32″W	2630 m	Ref. 10
6	KNR-178-48JPC	off Cape Hatteras, western North Atlantic	35°46′N 74°27′W	2009 m	Ref. 47
7	2010-GB2-MCA	Garrison Basin, northern Gulf of Mexico	26°40′11″N 93°55′13″W	1776 m	Ref. 14
8	Cuba Grande (CG) stalagmite	Dos Anos Cave, northwestern Cuba	22°23′N 83°58′W	100 m above sea level (cave)	Ref. 38
9	PDR-1 stalagmite	Perdida Cave, central Puerto Rico	18°N 67°W	350-400 m above sea level (cave)	Ref. 37
10	Pond sediment core (GT3)	Grape Tree Pond, Jamaica	17°53′37″N 76°37′06″W	1 m (pond)	Ref. 36
11	Lacustrine sediment core	Lake Punta Laguna, Yucatan Peninsula, southern Mexico	20°38′N 87°37′W	6 m (lake)	Ref. 33
12	YOK-I stalagmite	Yok Balum Cave, Yucatan Peninsula Belize	16°12′31″N 89°04′24″W	366 m above sea level (cave)	Ref. 35

Table S2. SST and SSS estimates for the Tobago Basin core-tops.

Core	M35003-6[a]	M35003-6[b]	M35/1-2-1[c]
Sample depth (cm)	0-0.5	0-1	0-1
G. ruber (white)	*sensu stricto*	n/a	*sensu lato*
Sediment fraction	>150 μm	355-400 μm	250-313 μm
Mg/Ca (mmol/mol) ±2σ	4.41±0.11	4.72±0.15	4.91±0.11
$\delta^{18}O$ (‰) ± 2σ	-1.83±0.14	-1.69±0.14	-1.93±0.16
SST (°C)[d] ±1σ	**26.70±0.33**	**27.99±0.33**	**28.02±0.46**
SSS (units)[d] ±1σ	**35.57±0.21**	**35.82±0.23**	**35.84±0.28**

[a] Mg/Ca and $\delta^{18}O$ values from this study
[b] Mg/Ca values from ref. 53, $\delta^{18}O$ values from ref. 71
[c] Mg/Ca and $\delta^{18}O$ values from ref. 21
[d] Based on paired Mg/Ca-$\delta^{18}O$ using PSU Solver (ref. 23, see Materials and Methods)

Table S3. Tie Points and Radiocarbon Age Control for core M35003-6.

Mid-Depth (cm)	Tie point (Yr. C.E.)	Lab Code for ^{14}C date	Conv. Age (Yr B.P.)	Median Probability Calendar Age* (Yr C.E.)	Calendar Age Range (2σ, Yr C.E./B.C.E.)
0.25	1996				
4.14	1853				
6.28	1612				
22.82	889				
28.45	749				
2.75		KIA 50748**	560±20	1853	1675-1981
10.25		KIA 50749**	795±20	1505	1225-1788
26.25		KIA 50750**	1440±20	852	519-1151
44.75		KIA 50751**	2200±25	31	-382-420

*Radiocarbon dates for all depths were calibrated in BACON (64).
**Radiocarbon dates were not used in the final age model, which was built on correlation to core 2010-GB2-MCA (4 tie points). In addition, modern age (1996 C.E.) was assumed for the core-top of M35003-6 (see supplementary text, fig. S2).

Table S4. Radiocarbon Age Control for core 2010-GB2-MCA.

Mid-Depth (cm)	Conv. Age (Yr B.P.)	BACON Median Probability Calendar Age (Yr C.E.)	Calendar Age Range (2σ, Yr C.E./B.C.E.)
0.25	>Modern±30*	1998	1936-2059
9.65	855±30	1475	1326-1642
19.25	1450±30	934	770-1105
34.75	2405±30	-124	-325-101

*Radiocarbon dates for all depths (from ref. 14) were re-calibrated in BACON (64) using the Marine20 ΔR database (ΔR=-164±9 years, ref. 66) and a Marine20 calibration curve (62), except for the core-top, for which a modern age was assumed.

REFERENCES AND NOTES

1. P. Braconnot, S. P. Harrison, M. Kageyama, P. J. Bartlein, V. Masson-Delmotte, A. Abe-Ouchi, B. Otto-Bliesner, Y. Zhao, Evaluation of climate models using palaeoclimatic data. *Nat. Clim. Change* **2**, 417–424 (2012).

2. U. Büntgen, V. S. Myglan, F. C. Ljungqvist, M. McCormick, N. Di Cosmo, M. Sigl, J. Jungclaus, S. Wagner, P. J. Krusic, J. Esper, J. O. Kaplan, M. A. C. de Vaan, J. Luterbacher, L. Wacker, W. Tegel, A. V. Kirdyanov, Cooling and societal change during the Late Antique Little Ice Age from 536 to around 660 AD. *Nat. Geosci.* **9**, 231–236 (2016).

3. V. Masson-Delmotte, M. Schulz, A. Abe-Ouchi, J. Beer, J. Ganopolski, J. F. González Rouco, E. Jansen, K. Lambeck, J. Luterbacher, T. Naish, T. Osborn, B. Otto-Bliesner, T. Quinn, R. Ramesh, M. Rojas, X. Shao, A. Timmermann, Information from paleoclimate archives. *Climate Change 2013: The Physical Science Basis. Contribution of Working Group I to the Fifth Assessment Report of the Intergovernmental Panel on Climate Change*. T. F. Stocker, D. Qin, G.-K. Plattner, M. Tignor, S. K. Allen, J. Doschung, A. Nauels, Y. Xia, V. Bex, and P. M. Midgley, Eds., (Cambridge Univ. Press, 2013), pp. 383–464.

4. M. E. Mann, Z. Zhang, S. Rutherford, R. S. Bradley, M. K. Hughes, D. Shindell, C. Ammann, G. Faluvegi, F. Ni, Global signatures and dynamical origins of the Little Ice Age and Medieval Climate Anomaly. *Science* **326**, 1256–1260 (2009).

5. R. Neukom, N. Steiger, J. J. Gómez-Navarro, J. Wang, J. P. Werner, No evidence for globally coherent warm and cold periods over the preindustrial Common Era. *Nature* **571**, 550–554 (2019).

6. P. Moffa-Sánchez, E. Moreno-Chamarro, D. J. Reynolds, P. Ortega, L. Cunningham, D. Swingedouw, J. Amrhein, J. Halfar, L. Jonkers, J. H. Jungclaus, K. Perner, A. Wanamaker, S. Yeager, Variability in the northern North Atlantic and Arctic Oceans across the last two millennia: A review. *Paleoceanogr. Paleoclimatol.* **34**, 1399–1436 (2019).

7. J. Slawinska, A. Robock, Impact of volcanic eruptions on decadal to centennial fluctuations of Arctic sea ice extent during the last millennium and on initiation of the little ice age. *J. Climate* **31**, 2145–67 (2018).

8. P. Moffa-Sánchez, A. Born, I. R. Hall, D. J. R. Thornalley, S. Barker, Solar forcing of North Atlantic surface temperature and salinity over the past millennium. *Nat. Geosci.* **7**, 275–278 (2014).

9. F. Lehner, A. Born, C. C. Raible, T. F. Stocker, Amplified inception of European Little Ice Age by sea ice–ocean–atmosphere feedbacks. *J. Climate* **26**, 7586–7602 (2013).

10. P. Moffa-Sánchez, I. R. Hall, North Atlantic variability and its links to European climate over the last 3000 years. *Nat. Commun.* **8**, 1726 (2017).

11. D. C. Lund, J. Lynch-Stieglitz, W. B. Curry, Gulf Stream density structure and transport during the past millennium. *Nature* **444**, 601–604 (2006).

12. A. D. Wanamaker Jr, P. G. Butler, J. D. Scourse, J. Heinemeier, J. Eiríksson, K. L. Knudsen, C. A. Richardson, Surface changes in the North Atlantic Meridional Overturning Circulation during the last millennium. *Nat. Commun.* **3**, 899 (2012).

13. D. J. Reynolds, J. D. Scourse, P. R. Halloran, A. J. Nederbragt, A. D. Wanamaker, P. G. Butler, C. A. Richardson, J. Heinemeier, J. Eiríksson, K. L. Knudsen, I. R. Hall, Annually resolved North Atlantic marine climate over the last millennium. *Nat. Commun.* **7**, 13502 (2016).

14. K. Thirumalai, T. M. Quinn, Y. Okumura, J. N. Richey, J. W. Partin, R. Z. Poore, E. Moreno-Chamarro, Pronounced centennial-scale Atlantic Ocean climate variability correlated with Western Hemisphere hydroclimate. *Nat. Commun.* **9**, 392 (2018).

15. F. Lapointe, R. S. Bradley, P. Francus, N. L. Balascio, M. B. Abbott, J. Stoner, G. St-Onge, A. De Coninck, T. Labarre, Annually resolved Atlantic sea surface temperature variability over the past 2,900 y. *Proc. Natl. Acad. Sci. U.S.A.* **117**, 27171–27178 (2020).

16. J. Nyberg, B. A. Malmgren, A. Kuijpers, A. A. Winter, A centennial-scale variability of tropical North Atlantic surface hydrography during the late Holocene. *Palaeogeogr. Palaeoclimatol. Palaeoecol.* **183**, 25–41 (2002).

17. K. H. Kilbourne, M. A. Alexander, J. A. Nye, A low latitude paleoclimate perspective on Atlantic multidecadal variability. *J. Mar. Sys.* **133**, 4–13 (2014).

18. J. E. Tierney, N. J. Abram, K. J. Anchukaitis, M. N. Evans, C. Giry, K. H. Kilbourne, C. P. Saenger, H. C. Wu, J. Zinke, Tropical sea surface temperatures for the past four centuries reconstructed from coral archives. *Paleoceanography* **30**, 226–252 (2015).

19. J. B. Wurtzel, D. E. Black, R. C. Thunell, L. C. Peterson, E. J. Tappa, S. Rahman, Mechanisms of southern Caribbean SST variability over the last two millennia. *Geophys. Res. Lett.* **40**, 5954–5958 (2013).

20. A. Zhuravleva, M. Hüls, R. Tiedemann, H. A. Bauch, A 125-ka record of northern South American precipitation and the role of high-to-low latitude teleconnections. *Quat. Sci. Rev.* **270**, 107159 (2021).

21. A. Bahr, J. Schönfeld, J. Hoffmann, S. Voigt, R. Aurahs, M. Kucera, S. Flögel, A. Jentzen, A. Gerdes, Comparison of Ba/Ca and δO^{18}_{WATER} as freshwater proxies: A multi-species core-top study on planktonic foraminifera from the vicinity of the Orinoco River mouth. *Earth Planet. Sci. Lett.* **383**, 45–57 (2013).

22. B. Schmuker, R. Schiebel, Planktic foraminifers and hydrography of the eastern and northern Caribbean Sea. *Mar. Micropaleontol.* **46**, 387–403 (2002).

23. K. Thirumalai, T. M. Quinn, G. Marino, Constraining past seawater $\delta^{18}O$ and temperature records developed from foraminiferal geochemistry. *Paleoceanography* **31**, 1409–1422 (2016).

24. K. Zhao, M. A. Wulder, T. Hu, R. Bright, Q. Wu, H. Qin, Y. Li, E. Toman, B. Mallick, X. Zhang, M. Brown, Detecting change-point, trend, and seasonality in satellite time series data to track abrupt changes and nonlinear dynamics: A Bayesian ensemble algorithm. *Remote Sens. Environ.* **232**, 111181 (2019).

25. A. Mora, A. Laraque, P. Moreira-Turcq, J. A. Alfonso, Temporal variation and fluxes of dissolved and particulate organic carbon in the Apure, Caura and Orinoco rivers, Venezuela. *J. South. Am. Earth Sci.* **54**, 47–56 (2014).

26. F. E. Müller-Karger, C. R. McClain, T. R. Fisher, W. E. Esaias, R. Varela, Pigment distribution in the Caribbean sea: Observations from space. *Prog. Oceanogr.* **23**, 23–64 (1989).

27. R. López, J. M. López, J. Morell, J. E. Corredor, C. E. del Castillo, Influence of the Orinoco River on the primary production of eastern Caribbean surface waters. *J. Geophys. Res. Oceans* **118**, 4617–4632 (2013).

28. C. Wang, L. Zhang, S. K. Lee, Response of freshwater flux and sea surface salinity to variability of the Atlantic warm pool. *J. Climate* **26**, 1249–1267 (2013).

29. C. Y. Da-Allada, G. Alory, Y. du Penhoat, E. Kestenare, F. Durand, N. M. Hounkonnou, Seasonal mixed-layer salinity balance in the tropical Atlantic Ocean: Mean state and seasonal cycle. *J. Geophys. Res. Oceans* **118**, 332–345 (2013).

30. C. Wang, D. B. Enfield, S. K. Lee, C. W. Landsea, Influences of the Atlantic Warm Pool on Western Hemisphere summer rainfall and Atlantic hurricanes. *J. Climate* **19**, 3011–3028 (2006).

31. T. Bhattacharya, J. C. H. Chiang, W. Cheng, Ocean-atmosphere dynamics linked to 800–1050 CE drying in Mesoamerica. *Quat. Sci. Rev.* **169**, 263–277 (2019).

32. L. Zhang, C. Wang, S. K. Lee, Potential role of Atlantic Warm Pool-induced freshwater forcing in the Atlantic Meridional Overturning Circulation: Ocean–sea ice model simulations. *Climate Dynam.* **43**, 553–574 (2014).

33. J. H. Curtis, D. A. Hodell, M. Brenner, Climate variability on the Yucatan Peninsula (Mexico) during the past 3500 years, and implications for Maya cultural evolution. *Quatern. Res.* **46**, 37–47 (1996).

34. M. Medina-Elizalde, E. J. Rohling, Collapse of classic Maya civilization related to modest reduction in precipitation. *Science* **335**, 956–959 (2012).

35. D. J. Kennett, S. F. M. Breitenbach, V. V. Aquino, Y. Asmerom, J. Awe, J. U. L. Baldini, P. Bartlein, B. J. Culleton, C. Ebert, C. Jazwa, M. J. Macri, N. Marwan, V. Polyak, K. M. Prufer, H. E. Ridley, H. Sodemann, B. Winterhalder, G. H. Haug, Development and disintegration of Maya political systems in response to climate change. *Science* **338**, 788–791 (2012).

36. M. J. Burn, S. E. Palmer, Solar forcing of Caribbean drought events during the last millennium. *J. Quat. Sci.* **29**, 827–836 (2014).

37. A. Winter, T. Miller, Y. Kushnir, A. Sinha, A. Timmermann, M. R. Jury, C. Gallup, H. Cheng, R. L. Edwards, Evidence for 800 years of North Atlantic multi-decadal variability from a Puerto Rican speleothem. *Earth Planet. Sci. Lett.* **308**, 23–28 (2011).

38. C. Fensterer, D. Scholz, D. Hoffmann, C. Spötl, J. M. Pajón, A. Mangini, Cuban stalagmite suggests relationship between Caribbean precipitation and the Atlantic Multidecadal Oscillation during the past 1.3 ka. *Holocene* **22**, 1405–1412 (2012).

39. G. H. Haug, K. A. Hughen, D. M. Sigman, L. C. Peterson, U. Röhl, Southward migration of the intertropical convergence zone through the Holocene. *Science* **293**, 1304–1308 (2001).

40. D. B. Enfield, A. M. Mestas-Nuñez, P. J. Trimble, The Atlantic multidecadal oscillation and its relation to rainfall and river flows in the continental U.S. *Geophys. Res. Lett.* **28**, 2077–2080 (2001).

41. A. R. Friedman, G. Reverdin, M. Khodri, G. Gastineau, A new record of Atlantic sea surface salinity from 1896 to 2013 reveals the signatures of climate variability and long-term trends. *Geophys. Res. Lett.* **44**, 1866–1876 (2017).

42. D. L. R. Hodson, P.-A. Bretonnière, C. Cassou, P. Davini, N. P. Klingaman, K. Lohmann, J. Lopez-Parages, M. Martín-Rey, M.-P. Moine, P.-A. Monerie, D. A. Putrasahan, C. D. Roberts, J. Robson, Y. Ruprich-Robert, E. Sanchez-Gomez, J. Seddon, R. Senan, Coupled climate response to Atlantic multidecadal variability in a multi-model multi-resolution ensemble. *Climate Dynam.* **59**, 805–836 (2022).

43. D. Zhang, R. Msadek, M. J. McPhaden, T. Delworth, Multidecadal variability of the North Brazil Current and its connection to the Atlantic meridional overturning circulation. *J. Geophys. Res. Oceans* **116**, C04012 (2011).

44. P. del Monte-Luna, H. Villalobos, F. Arreguín-Sánchez, Variability of sea surface temperature in the southwestern Gulf of Mexico. *Cont. Shelf Res.* **102**, 73–79 (2015).

45. W. E. Johns, T. L. Townsend, D. M. Fratantoni, W. Wilson, On the Atlantic inflow to the Caribbean Sea. *Deep Sea Res. I Oceanogr. Res. Pap.* **49**, 211–243 (2002).

46. E. Moreno-Chamarro, D. Zanchettin, K. Lohmann, J. H. Jungclaus, An abrupt weakening of the subpolar gyre as trigger of Little Ice Age-type episodes. *Clim. Dynam.* **48**, 727–744 (2017).

47. D. J. R. Thornalley, D. W. Oppo, P. Ortega, J. I. Robson, C. M. Brierley, R. Davis, I. R. Hall, P. Moffa-Sanchez, N. L. Rose, P. T. Spooner, I. Yashayaev, L. D. Keigwin, Anomalously weak Labrador Sea convection and Atlantic overturning during the past 150 years. *Nature* **556**, 227–230 (2018).

48. Ø. Hammer, D. A. T. Harper, P. D. Ryan, PAST: Paleontological statistics software package for education and data analysis. *Palaeontol. Electron.* **4**, 9 (2001).

49. M. Mohtadi, M. Prange, D. W. Oppo, R. De Pol-Holz, U. Merkel, X. Zhang, S. Steinke, A. Lückge, North Atlantic forcing of tropical Indian Ocean climate. *Nature* **509**, 76–80 (2014).

50. S. Barker, M. Greaves, H. Elderfield, A study of cleaning procedures used for foraminiferal Mg/Ca paleothermometry. *Geochem. Geophys. Geosyst.* **4**, 8407 (2003).

51. W. R. Gray, S. Weldeab, D. W. Lea, Y. Rosenthal, N. Gruber, B. Donner, G. Fischer, The effects of temperature, salinity, and the carbonate system on Mg/Ca in Globigerinoides ruber (white): A global sediment trap calibration. *Earth Planet. Sci. Lett.* **482**, 607–620 (2018).

52. W. R. Gray, D. Evans, Nonthermal influences on Mg/Ca in planktonic foraminifera: A review of culture studies and application to the last glacial maximum. *Paleoceanogr. Paleoclimatol.* **34**, 306–315 (2019).

53. M. Regenberg, D. Nürnberg, S. Steph, J. Groeneveld, D. Garbe-Schönberg, R. Tiedemann, W.-C. Dullo, Assessing the effect of dissolution on planktonic foraminiferal Mg/Ca ratios: Evidence from Caribbean core tops. *Geochem. Geophys. Geosyst.* **7**, 10.1029/2005GC001019 (2006).

54. B. Kısakürek, A. Eisenhauer, F. Böhm, D. Garbe-Schönberg, J. Erez, Controls on shell Mg/Ca and Sr/Ca in cultured planktonic foraminiferan, Globigerinoides ruber (white). *Earth Planet. Sci. Lett.* **273**, 260–269 (2008).

55. B. E. Bemis, H. J. Spero, J. Bijma, D. W. Lea, Reevaluation of the oxygen isotopic composition of planktonic foraminifera: Experimental results and revised paleotemperature equations. *Paleoceanography* **13**, 150–160 (1998).

56. A. N. LeGrande, G. A. Schmidt, Global gridded data set of the oxygen isotopic composition in seawater. *Geophys. Res. Lett.* **33**, L12604 (2006).

57. F. Fatela, R. Taborda, Confidence limits of species proportions in microfossil assemblages. *Mar. Micropaleontol.* **45**, 169–174 (2002).

58. H. Zuo, M. A. Balmaseda, S. Tietsche, K. Mogensen, M. Mayer, The ECMWF operational ensemble reanalysis–analysis system for ocean and sea ice: A description of the system and assessment. *Ocean Sci.* **15**, 779–808 (2019).

59. T. P. Boyer, J. I. Antonov, O. K. Baranova, H. E. Garcia, D. R. Johnson, A. V. Mishonov, T. D. O'Brien, D. Seidov, I. Smolyar, M. M. Zweng, C. R. Paver, World ocean database 2013 (2013).

60. R. Schlitzer, Ocean Data View; https://odv.awi.de (2018).

61. J. N. Richey, K. Thirumalai, D. Khider, C. E. Reynolds, J. W. Partin, T. M. Quinn, Considerations for Globigerinoides ruber (white and pink) paleoceanography: Comprehensive insights from a long-running sediment trap. *Paleoceanogr. Paleoclimatol.* **34**, 353–373 (2019).

62. T. J. Heaton, P. Köhler, M. Butzin, E. Bard, R. W. Reimer, W. E. Austin, C. B. Ramsey, P. M. Grootes, K. A. Hughen, B. Kromer, P. J. Reimer, J. Adkins, A. Burke, M. S. Cook, J. Olsen, L. C. Skinner, Marine20—The marine radiocarbon age calibration curve (0–55,000 cal BP). *Radiocarbon* **62**, 779–820 (2020).

63. R. J. DiNapoli, S. M. Fitzpatrick, M. F. Napolitano, T. C. Rick, J. H. Stone, N. P. Jew, Marine reservoir corrections for the Caribbean demonstrate high intra- and inter-island variability in local reservoir offsets. *Quat. Geochronol.* **61**, 101126 (2021).

64. M. Blaauw, J. A. Christen, Flexible paleoclimate age-depth models using an autoregressive gamma process. *Bayesian Anal.* **6**, 457–474 (2011).

65. T. P. Guilderson, J. E. Cole, J. R. Southon, Pre-bomb Δ14C variability and the suess effect in cariaco basin surface waters as recorded in hermatypic corals. *Radiocarbon* **47**, 57–65 (2005).

66. A. J. Wagner, T. P. Guilderson, N. C. Slowey, J. E. Cole, Pre-bomb surface water radiocarbon of the Gulf of Mexico and Caribbean as recorded in hermatypic corals. *Radiocarbon* **51**, 947–954 (2009).

67. G. Rodriguez-Vera, R. Romero-Centeno, C. L. Castro, V. M. Castro, Coupled interannual variability of wind and sea surface temperature in the Caribbean sea and the Gulf of Mexico. *J. Climate* **32**, 4263–4280 (2019).

68. K. M. Yeager, P. H. Santschi, G. T. Rowe, Sediment accumulation and radionuclide inventories (239,240Pu, 210Pb and 234Th) in the northern Gulf of Mexico, as influenced by organic matter and macrofaunal density. *Mar. Chem.* **91**, 1–14 (2004).

69. M. H. Trauth, M. Sarnthein, M. Arnold, Bioturbational mixing depth and carbon flux at the seafloor. *Paleoceanography* **12**, 517–526 (1997).

70. M. Hüls, R. Zahn, Millennial-scale sea surface temperature variability in the western tropical North Atlantic from planktonic foraminiferal census counts. *Paleoceanography* **15**, 659–678 (2000).

71. S. Steph, M. Regenberg, R. Tiedemann, S. Mulitza, D. Nürnberg, Stable isotopes of planktonic foraminifera from tropical Atlantic/Caribbean core-tops: Implications for reconstructing upper ocean stratification. *Mar. Micropaleontol.* **71**, 1–19 (2009).